Int J Adv Manuf Technol (2016) 87:2745–2762
DOI 10.1007/s00170-016-8667-4

ORIGINAL ARTICLE

Influence of process parameters on kerf geometry and surface roughness in Nd:YAG laser cutting of Al 6061T6 alloy sheet

C. Leone[1,2] · S. Genna[2] · A. Caggiano[3,4] · V. Tagliaferri[2,5] · R. Molitierno[6]

Received: 11 December 2015 / Accepted: 22 March 2016 / Published online: 2 April 2016

Abstract In the present study, fine laser cutting of aluminium alloy 6061-T6 sheets, characterised by light reflection and heat conductivity, by means of a 150-W multimode lamp pumped Nd:YAG laser is investigated through an experimental testing campaign. Design of experiments (DoE) and analysis of variance (ANOVA) are adopted to study the influence of the process parameters on the kerf geometry and surface roughness. The results show that the laser allows cutting 1-mm-thick AA6061-T6 sheets with a cutting speed up to 700 mm/min, obtaining narrow kerfs (smaller than 200 μm), a fine taper angle (lower than 4°), a low dross height (about 40 μm) and a roughness average, Ra, around 4 μm.

Keywords Pulsed laser · Aluminium alloy 6061 · Kerf geometry · Roughness · ANOVA · Design of experiments

✉ C. Leone
claleone@unina.it

[1] Department of Industrial and Information Engineering, Second University of Naples, Via Roma 29, 81031 Aversa (Ce), Italy

[2] CIRTIBS Research Centre, University of Naples Federico II, P.le Tecchio 80, 80125 Naples, Italy

[3] Department of Chemical, Materials and Industrial Production Engineering, University of Naples Federico II, P.le Tecchio 80, 80125 Naples, Italy

[4] Fraunhofer Joint Laboratory of Excellence on Advanced Production Technology, P.le Tecchio 80, 80125 Naples, Italy

[5] Department of Enterprise Engineering, University of Rome Tor Vergata, Via del Politecnico 1, 00133 Rome, Italy

[6] MBDA Italia Spa, Via Calosi 1, 80070 Bacoli (NA), Italy

1 Introduction

Aluminium alloys are widely used in several advanced manufacturing industries due to their unique performance related to light weight, high strength and stiffness to weight ratio, high corrosion resistance and high thermal and electrical conductivity, non-toxicity and ease of formability and machinability [1, 2]. Thanks to their properties, these alloys found their main applications in aerospace components, automotive and maritime applications, electrical appliances, consumer durable, portable tools and sport equipments [2].

Aluminium alloys can be easily cut through a number of different material removal processes, such as punching, machining (profiling), abrasive water jet and electrical discharge machining. However, when small and complex 2D geometries with high productivity are required, the most common, flexible and fast process for cutting is represented by laser beam cutting (LBC) [3, 4]. Compared to traditional technologies, laser machining offers several benefits such as the absence of mechanical contact and tool wear, no need for complex fixtures and the possibility to create complex shapes and accurate geometries with narrow kerfs on almost all categories of materials including metals, non-metals, ceramics and composites [5–13]. Laser cutting processes are based on a thermal interaction: when the beam radiates the material, part of the laser radiation is absorbed causing melting, vaporization or chemical state change of the material which can be easily removed by a pressurized assistant gas jet. The material removal rate (MRR) and the kerf profile characteristics (geometry, roughness and heat-affected zone) are a function of the process parameters, such as the type of adopted source (including the wavelength and the beam quality), the average power, the cutting speed, the focus position and the beam spot dimension, the type of assistant gas and its pressure. Moreover, in case of pulsed laser sources, the MRR and kerf

Table 1 Laser system characteristics

Characteristic	Symbol	Value	Units
Wavelength	λ	1064	[nm]
Average nominal power	Pa	150	[W]
Pulse duration	D	0.03÷2.5	[ms]
Pulse frequency	F	up to 3	[kHz]
Mode	–	Multimode	–
Beam polarization	–	random	–
Beam diameter (at the resonator exit)	–	6	[mm]
Beam expander	–	3X	–
Focal length of focussing lens	–	80	[mm]
Focused spot diameter	ds	≈170	[μm]

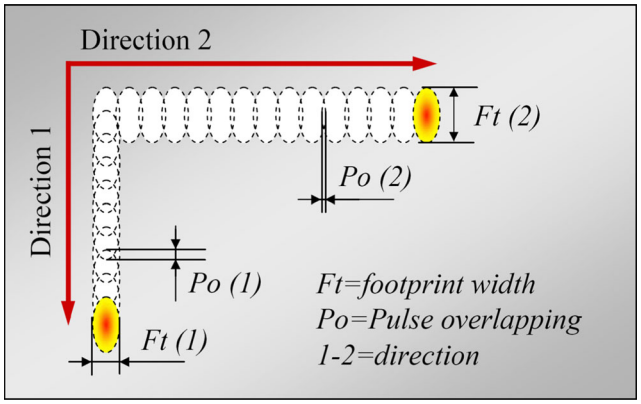

Fig. 2 Effect of the elliptical spot shape on the overlapping factor and on the kerf width depending on the beam travel direction.

characteristics are also influenced by the pulse frequency, the pulse duration and the overlapping percentage. The effects of the process parameters on the kerf characteristics have been widely studied in the past. In [14, 15], the influence of power and cutting speed in laser cutting of different steels adopting a CO_2 laser source was studied. It was found that the kerf width increases when increasing the laser power and decreasing the cutting speed. Moreover, in [14], it was found that the adoption of a reactive gas (oxygen or air) as assistant gas, instead of an inert gas, leads to a wider kerf and higher roughness. Also, the focus position influences the kerf geometry; in [16], it was found that the minimum kerf width is obtained by setting the focus on the workpiece surface for thin sheets (<1.5 mm) and inside the workpiece for thicker sheets (>1.5).

Compared to the CO_2 laser source, Nd:YAG lasers show a lower average power. However, when operating in pulsed mode, they are able to yield pulses characterized by high peak power. This feature, together with the shorter and better absorbed wavelength, allows these lasers to cut the same materials with a lower average power compared to CO_2 sources

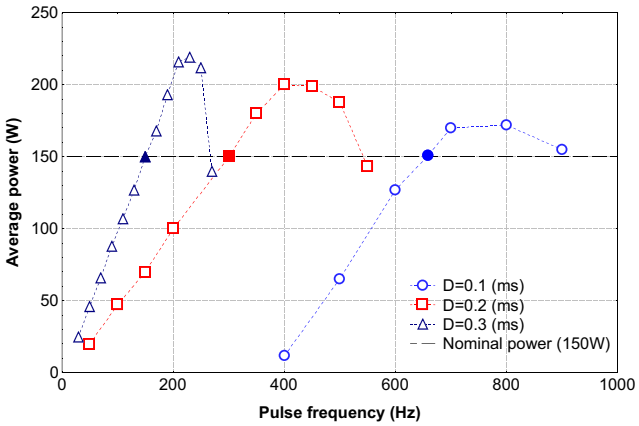

Fig. 1 Average power against pulse frequency at different pulse durations. Data obtained with a lamp voltage of 700 V. The *filled dots* represent the adopted frequency

[1, 16–19]. Consequently, Nd:YAG lasers are suitable for processing of metals in general and reflective materials in particular.

Regarding the effect of the pulse parameters, in [20], a study on the influence of process parameters during Nd:YAG laser drilling of Ni-based superalloy sheet, 1 mm in thickness, was presented. In the study, it was found that a spot overlap increase produces an enlargement of the kerf, while a short pulse duration allows for a low kerf taper angle, if compared to a longer duration pulse. These results are consistent to what observed in similar studies on laser cutting of stainless steel [15, 21].

In the literature, there are a limited number of papers on laser cutting of aluminium adopting both CO_2 and Nd:YAG laser sources [1, 22–26]. Many of them concern cutting of 2-xxx, 4-xxx or 5-xxx alloy series, while no studies on the 6-xxx alloy series are reported.

Unlike standard-grade or carbon steel, aluminium alloys are light-reflective and heat-conductive metals. High reflectivity means that a high power density is required to initiate cutting. High thermal conductivity means that the heat is transported from the cutting front rapidly, which can lead to difficulties when initiating the cut. Consequently, the maximum cutting speed is reduced. Moreover, the ease with which the aluminium is oxidized is a source for further problems: in oxygen-assisted cutting, the variation in the oxide layer thickness along the cutting line and on the cutting front results in a variation of material absorbance and then in crater irregularity, rough cut edge and dross formation [27]. Not even the use of inert gases, such as nitrogen, may solve this problem. In this case, the cooling effect of the gas together with the high thermal conductivity tends to shed heat, especially between two consecutive pulses. Consequently, the molten material pushed by the assistant gas, cools inside and at the bottom of the kerf. As a result, the kerf is characterised by a recast layer, high taper angle, striations and dross at the kerf exit.

Table 2 Chemical composition and properties of Al6061-T6 [34]

Element	Al	Mg	Si	Cr	Mn
Min [%]	95.8	0.8	0.4	0.04	–
Max [%]	98.6	1.2	0.8	0.35	0.15
Element	Cu	Fe	Zn	Ti	Other
Min [%]	0.15	–	–	–	–
Max [%]	0.4	0.7	0.25	0.15	0.05
Properties			Value		Units
Density			2.7		[g/cm^3]
Melting range:					
Solidus temperature			582		[°C]
Liquidus temperature			652		[°C]
Specific heat			0.896		[J/kg, °C]
Thermal conductivity			167		[W/m°C]
Tensile strength			310		[MPa]
Yield strength (at 0.2 %)			276		[MPa]
Elongation			12–17		[%]
Young's modulus			68.9		[GPa]

Concerning striations, they are periodic lines appearing on the cut surface, which affects the surface, appearance and geometrical accuracy of laser cutting. The presence of striations is undesirable since they may act as stress raisers in addition to the unpredictable geometric changes, calling for further finishing operations to achieve a smooth surface [28]. The formation of striations involves complex mechanisms, not completely understood yet. Many studies have been carried out to investigate the mechanism of striations formation [29–31]. Miyamoto and Maruo [29] had firstly explained these striation lines through the model of ignition-extinction cycle. Ivarson et al. [30] explained that the most likely sources of striations formation are as follows: (i) a cyclic variation in the driving force of the oxidation reaction, the variation being brought about by changes in the oxygen partial pressure in the cut zone melt, and (ii) viscosity and surface tension effects associated with melt removal. Moreover, these phenomena are due to one or more of the following mechanisms: molten solidification process; gas dynamics; melt boiling; optical effects; time-based fluctuations of power input, etc. The curvature of the striation lines matches the curvature of the laser beam cut front and so the inclination occurs when the energy flux velocity equals the cutting rate. Since in continuous regime (CW) laser sources the striations are due to periodic phenomena, even more so, it is expected that these are formed when the laser works in pulsed regime (PW). In [31], Kim et al. showed that the laser power intensity is the most important factor in the formation of striation patterns, since it is the most influential in the heating of metal and the formation of striations is caused by the ejection of molten metal and evaporation during laser cutting process. They showed that high laser power resulted in clear regular striation pattern, while relatively low power density caused the formation of a hot spot, which hindered the formation of regular striation patterns and caused less striation.

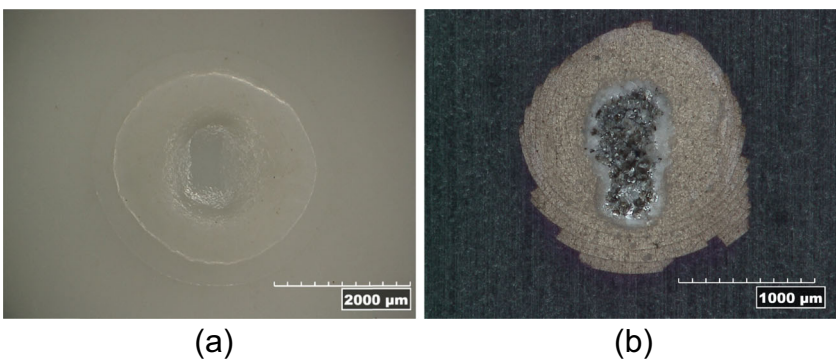

Fig. 3 Images of footprint obtained at D = 0.3 ms, F = 150 Hz, Pa = 150 W, on: **a** grey polypropylene (PP); **b** black anodised aluminium

Table 3 Process conditions adopted for the evaluation of the maximum cutting speed (Sl)

Control factors	Labels	Low (−)	Middle (0)	High (+)	Unit
Direction	Dr	1	–	2	–
Duration	D	0.1	0.2	0.3	[ms]
Cutting speed	Cs		up to incomplete cut		

Therefore, particular attention must be paid to ensure an adequate quality of the laser cut. Possible solutions involve the use of a higher power source or pulsed sources (with high pulse power) coupled with assistant gas at a pressure in the range 5–17 bar that helps the removal of molten material.

Moreover, the pulsed Nd:YAG laser sources are often characterised by a low quality beam, such as multimode profile, high M^2 factors resulting in a beam parameter product in the range 10–80 mm · mrad, characteristics that are more evident for high power laser sources or when the source is a lamp pumped one [32]. This, often, results in an irregular energy distribution within the laser beam, which modifies the cut characteristics as a function of the cutting direction [33]. This aspect is generally neglected in research; however, it becomes essential in real applications, especially when small and complex 2D geometries, tight tolerances, perpendicular surfaces and absence of burr or recast layer are required.

In this research work, laser cutting of aluminium 6061-T6 sheets through the employment of a 150 W multimode pulsed Nd:YAG laser is investigated. Two experimental test series were carried out. At first, linear scans were executed using the maximum average power (150 W) and different cutting directions and pulse durations. On the basis of these tests, the maximum cutting speeds were determined. In the second experimental test series, cutting tests were performed by varying the beam travel direction, the duration and the cutting speed (selected as a percentage of the maximum cutting speed). The obtained kerfs sections were investigated by optical analysis. The top kerf, bottom kerf, taper angle, the angularity tolerance and dross height were measured. Moreover, the roughness along the cutting surface were acquired and analysed. Analysis of variance (ANOVA) was applied in order to study the influence of the process parameters on the kerf geometry and quality.

Table 4 Control factors and levels adopted in the kerf analysis tests

Control factors	Labels	Low (−)	Middle (0)	High (+)	Unit
Direction	Dr	1	–	2	–
Speed limit	Sl	80	90	100	[%]
Duration	D	0.1	–	0.3	[ms]

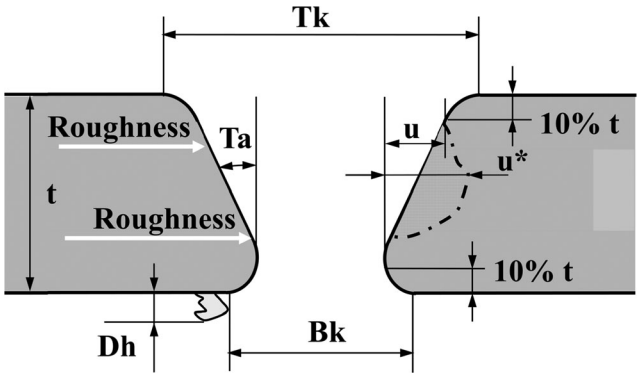

Fig. 4 Definition of kerf geometry parameters (UNI EN ISO 12584)

2 Experimental setup

2.1 Equipment

The experimental tests were performed using a 150 W lamp pumped Nd:YAG laser (Rofin Starcut 150). The laser beam was moved by means of a CNC system (Rofin finecut Y 340M). A cutting head (Precitek AK-YK 52), equipped with a lens having a focal length of 80 mm, was mounted on the system. In this way, a theoretical spot of about 170 μm was obtained. The system controls the generation of the geometric patterns, the cutting speed (Cs) and the laser source process parameters: lamp voltage (V), pulse duration (D) and pulse frequency (F). Table 1 shows the detailed characteristics of the laser system. Fixed the lamp voltage at the maximum value, the average power (Pa) depends on the adopted values of D and F, as reported in Fig. 1. The average power was measured using a power meter (F150A-SH thermal head and NOVA display by OPHIR). By observing Fig. 1, it can be noticed that, for a fixed pulse duration, average power increases according to the increase of pulse frequency till the maximum value. From there on, a decrease of average power is seen. It is

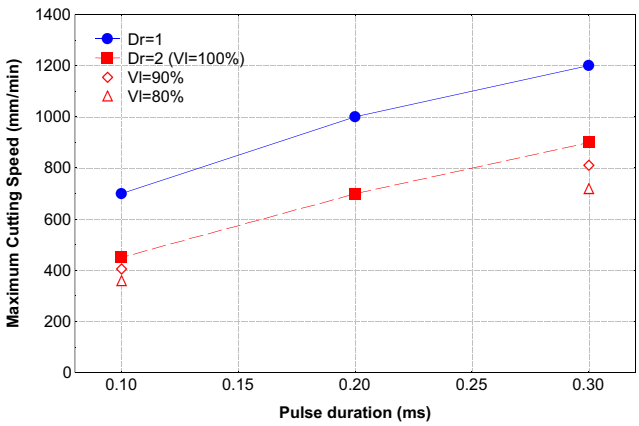

Fig. 5 The open dots represent the cutting speed adopted in the second testing series

Table 5 Process parameters, maximum cutting speed and the absolute values of the Sl adopted for the second experimental test

D	F	Pp	Ep	Cutting speed [mm/min]		
[ms]	[Hz]	[kW]	[J]	100 % Sl	90 % Sl	80 % Sl
0.3	150	3.33	1.00	900	810	720
0.1	659	2.28	0.23	450	405	360

reasonable to suppose that the power decrease is due by the pumping system saturation (i.e. power supply + lamp).

In this type of laser, the selection of the process parameters is a critical issue because the maximum cutting speed depends not only on the average power but also on pulse energy (Pe) and pulse power (Pp) [6, 7, 11, 12]. Furthermore, Pe and Pp play a central role in laser machining and micromachining as they determine, together with the focus spot, the fluence (energy density) and the irradiance (power density) and so the laser beam-material interaction mode, the amount of machined volume and the kerf geometry [3–13, 25, 26]. Pe and Pp depend on the process parameters Pa, D and F according to the well known equations [17–19].

$$Pe = Pa/F \tag{1}$$

$$Pp = Pe/D = Pa/(F{\cdot}D) \tag{2}$$

At the same time, it is worth noting that frequency (F), in conjunction with cutting speed (Cs), controls the superposition of two pulses in the space and time domains, the so-called overlapping, that is an additional critical parameter for pulse laser applications.

The overlapping percentage can be calculated through the following equation:

$$R\% = [1-(Cs/F{\cdot}ds)]{\cdot}100 \tag{3}$$

where ds is the spot diameter on the components.

In the adopted laser system, due to the multimode nature of the source, the energy intensity distribution in the laser spot is quasi-elliptical. As a result, the overlapping factor and the beam footprint width vary along with the beam travel direction, as visible in Fig. 2. Accordingly, a certain influence of the beam travel direction on the kerf geometry and quality is expected.

2.2 Material

The investigated material is aluminium 6061-T6 (UNS A96061; ISO AlMg1SiCu, AA6061-T6) in the form of 1 mm thick rolled sheets. AA6061 is a precipitation hardening aluminium alloy containing magnesium and silicon as major alloying elements. This alloy is of particular interest for advanced industries in sectors like aerospace, automotive, marine, electrical, chemical, food processing and sport equipments. It is characterized by high strength, medium fatigue strength and a very good corrosion resistance. In addition, it is weldable although strength is reduced in the weld zone. In

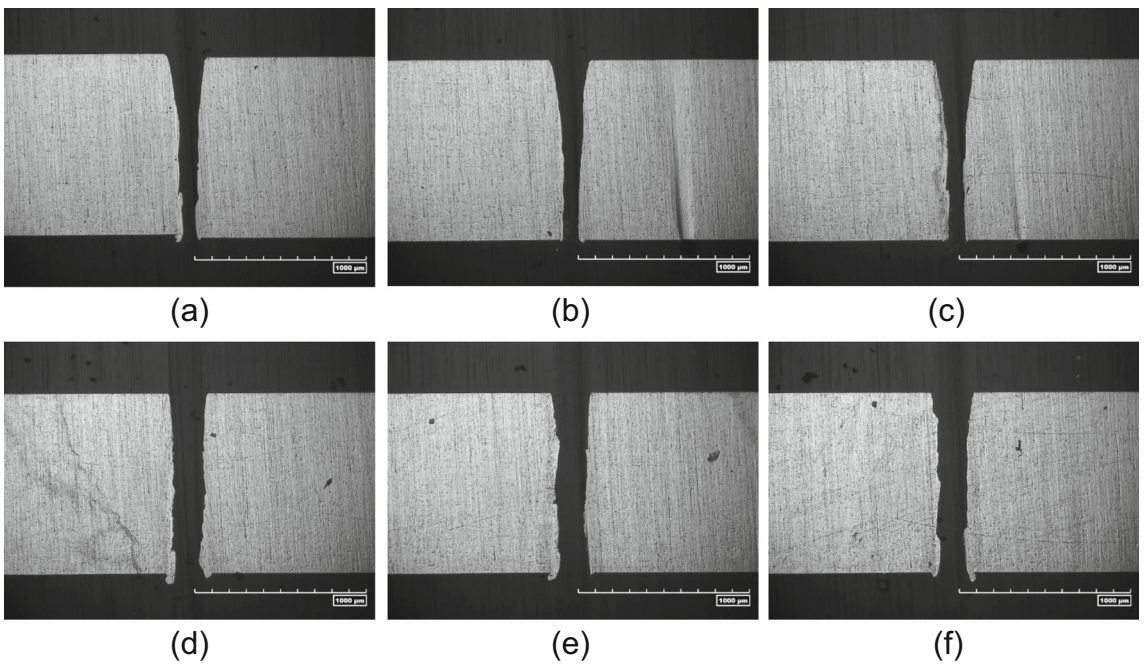

Fig. 6 Sections of the kerf obtained along direction 1 at different process condition: **a** Sl = 100 %, D = 0.1 ms; **b** Sl = 90 %, D = 0.1 ms; **c** Sl = 80 %, D = 0.1 ms; **d** Sl = 100 %, D = 0.3 ms; **e** Sl = 90 %, D = 0.3 ms; **f** Sl = 80 %, D = 0.3 ms

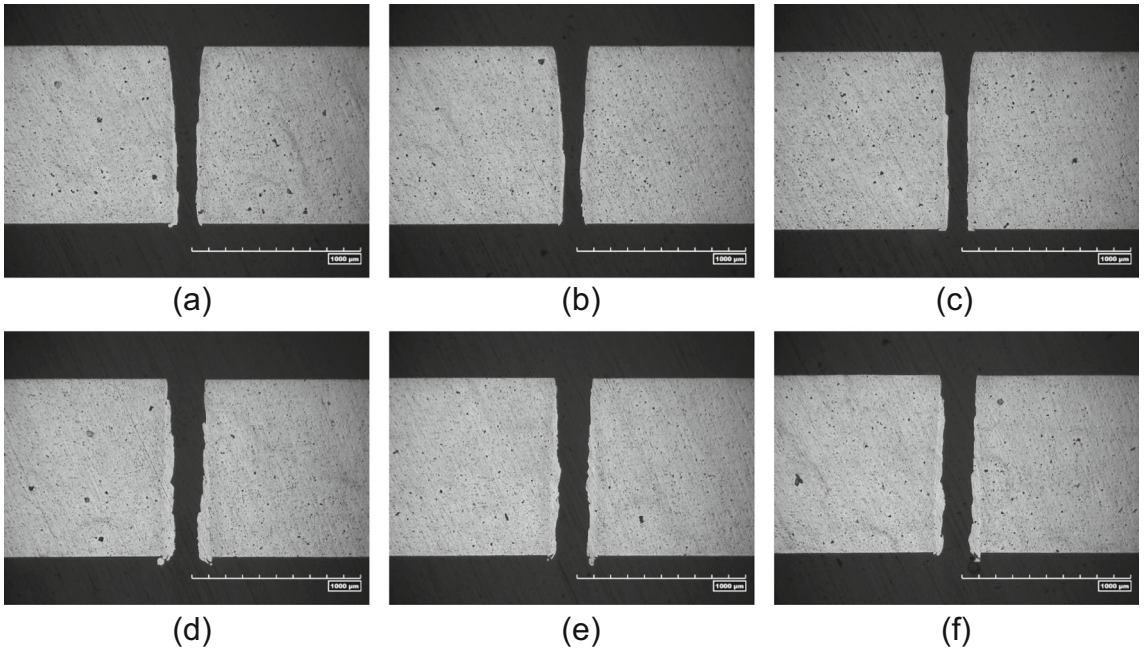

Fig. 7 Sections of the kerf obtained along direction 2 at different process condition: **a** Sl = 100 %, D = 0.1 ms; **b** Sl = 90 %, D = 0.1 ms; **c** Sl = 80 %, D = 0.1 ms; **d** Sl = 100 %, D = 0.3 ms; **e** Sl = 90 %, D = 0.3 ms; **f** Sl = 80 %, D = 0.3 ms

Table 2, the chemical composition and the main properties of the AA6061-T6 alloy are reported [34].

2.3 Experimental procedure

Two experimental testing series were performed. First, to obtain the maximum cutting speed, i.e. the speed beyond which it is not possible to cut the sheet (Sl), 30 mm long linear scans were carried out with the laser beam focused on the surface and maximum average power (150 W) while varying beam travel speed, pulse duration and beam direction.

For these tests, the process parameters were selected according to the above-mentioned considerations made on Pe and Pp. In particular, duration was chosen so as to take into

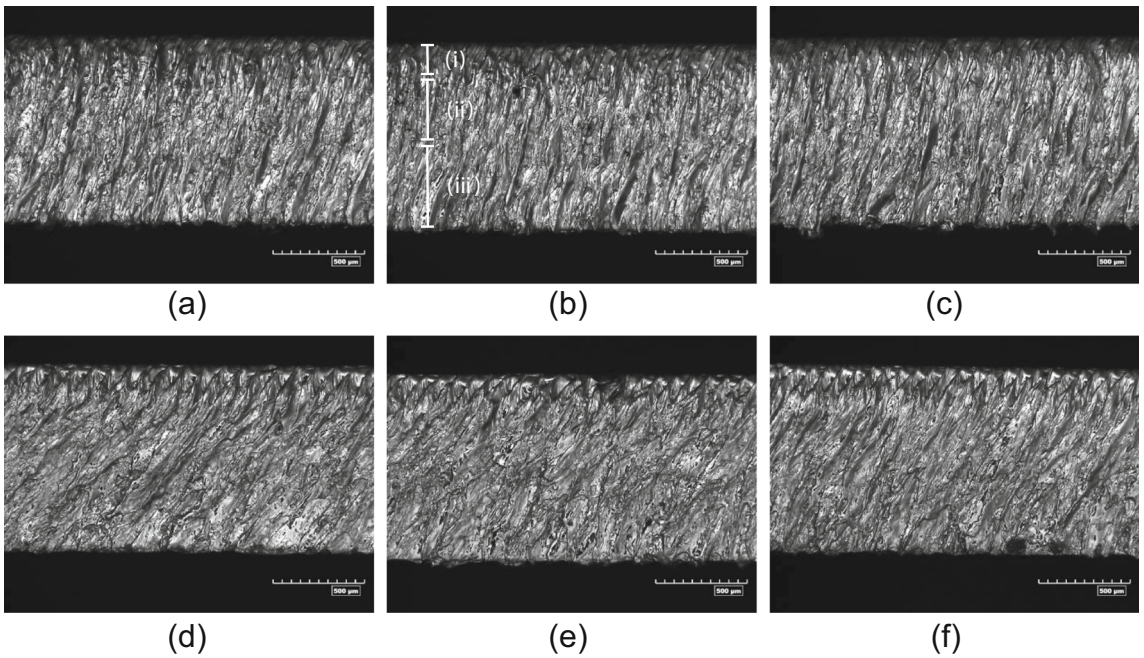

Fig. 8 Sections of the kerf obtained along direction 1 at different process condition: **a** Sl = 100 %, D = 0.1 ms; **b** Sl = 90 %, D = 0.1 ms; **c** Sl = 80 %, D = 0.1 ms; **d** Sl = 100 %, D = 0.3 ms; **e** Sl = 90 %, D = 0.3 ms; **f** Sl = 80 %, D = 0.3 ms

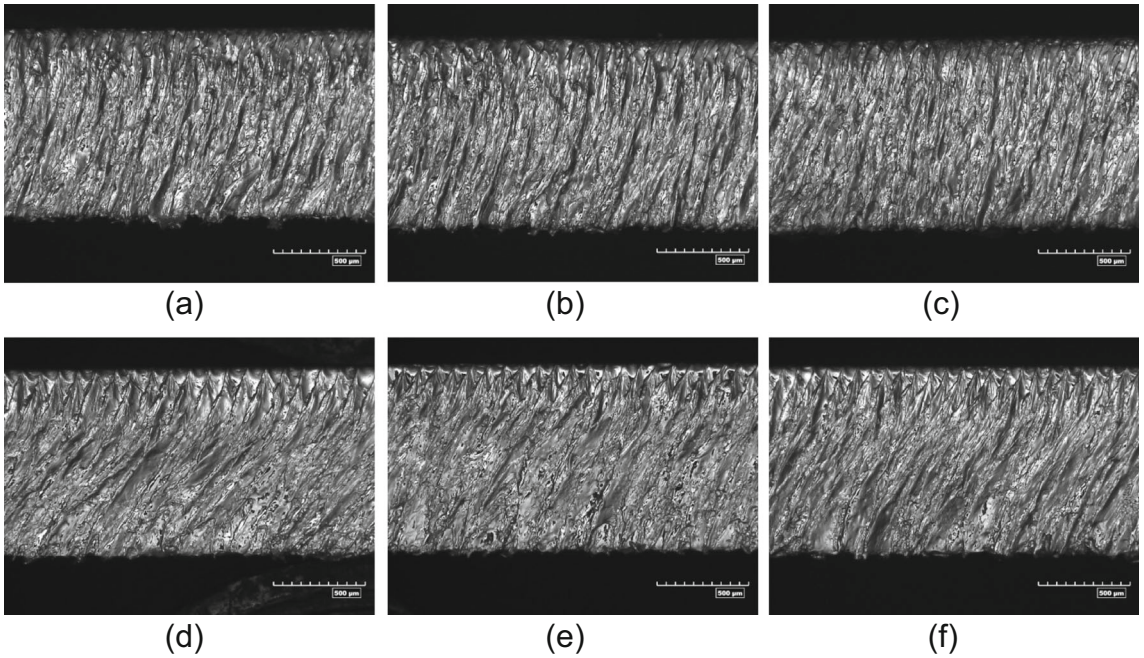

Fig. 9 Sections of the kerf obtained along direction 2 at different process condition: **a** Sl = 100 %, D = 0.1 ms; **b** Sl = 90 %, D = 0.1 ms; **c** Sl = 80 %, D = 0.1 ms; **d** Sl = 100 %, D = 0.3 ms; **e** Sl = 90 %, D = 0.3 ms; **f** Sl = 80 %, D = 0.3 ms

account the possible influence of Pe or Pp on the process. Therefore, in this first phase, three different values of duration were adopted and the pulse frequency was selected in order to have an average power (Pa) equal to the nominal value (150 W). On the other hand, the direction was chosen so as to take into account the effect of the energy distribution within the beam. In order to recognize the two directions where the beam width is the highest and the lowest, respectively, beam footprint was obtained on a grey polypropylene (PP) sheet, keeping the laser beam switched on at D = 0.3 ms, F = 150 Hz, Pa = 150 W for a sufficient time to achieve a suitable footprint. The test was repeated on a black anodised aluminium sheet. The footprints are reported in Fig. 3a, b, respectively. In both cases, a quasi-elliptical mark clearly appears in the centre of the footprint, due to the multimode laser beam spatial intensity distribution. Then, according to Fig. 2, the direction where the internal part of the footprint width was the lowest was assumed as direction 1, and the one where the mark width was the largest was assumed as direction 2. In Table 3, the process parameters adopted for the evaluation of the maximum cutting speed are reported. Moreover, nozzle diameter (1 mm), nozzle standoff distance (0.2 mm), focusing position (on sample surface), gas (nitrogen) and pressure (10 bar) were kept constant throughout the experimentation.

Afterwards, a second testing series was performed to verify the influence of the process parameters on the kerf geometry. For this experimental phase, a $2^2 \times 3$ full factorial design was developed according to the design of experiments (DoE) methodology. Compared to the typical approaches "one-factor-at-a-time", this kind of approach has the advantage to

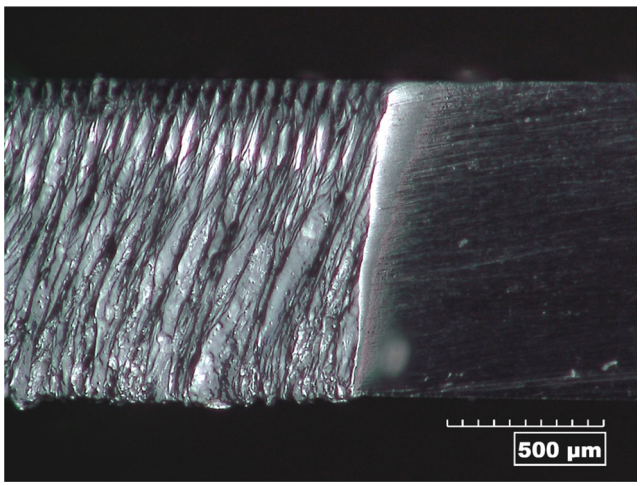

Fig. 10 Images of the corner obtained by the intersection of the cutting profile and normal section of a kerf. Sample obtained at Sl = 80 %, D = 0.3 ms, Dr = 2

Table 6 Computed values of kerf geometry response variables

	Tk [mm]	Bk [mm]	Ta [deg]	u [mm]	Dh [mm]
Mean	0.227	0.135	2.63	0.045	0.030
St. dev.	0.021	0.037	1.41	0.012	0.013
Max	0.280	0.200	5.60	0.072	0.063
Min	0.197	0.074	0.23	0.022	0.011

Table 7 Computed values of surface quality (roughness) response variables

	Ra_T [μm]	Rt_T [μm]	RSm_T [mm]	Ra_B [μm]	Rt_B [μm]	RSm_B [mm]
Mean	3.42	25.22	0.10	4.63	33.81	0.16
St. dev.	0.57	3.80	0.02	0.64	8.53	0.03
Max	4.96	33.50	0.16	6.78	74.30	0.21
Min	2.51	17.40	0.07	3.66	23.00	0.11

reduce the experimental runs necessary to investigate the effect of all the parameters and is able to provide information about the effects of the interaction between the various process parameters [12, 26, 35–37]. The following control factors were adopted: duration, maximum cutting speed and beam travel direction. In particular, it was chosen to adopt a scanning speed corresponding to the 100, 90 and 80 % of the minimum Sl measured for the two directions and for each duration. These conditions were adopted considering the effect of duration described below and the fact that, from a practical point of view, neither it is conceivable to use the highest speed (which would not assure to cut through the sheet along all the directions) nor to change the speed along the cutting direction. For each condition, four replications were executed. Table 4 summarizes the control factors and their settings.

It is worth noting that, under actual production conditions, the direction is not a selectable parameter. From a statistical point view, therefore, it would be more correct to use it as a covariate, rather than as a control factor. However, the use of a covariate would not allow to highlight the effect of the energy distribution within the beam and, above all, the interaction with the other control factors. Consequently, the understanding of the phenomena occurring during the laser cutting process might become difficult.

In order to determine which of the process parameters affect the kerf characteristics and how, ANOVA was used. The analysis was carried out at a 95 % confidence level ($\alpha = 0.05$), and the p-value was used to determine the significance of the factors or their combinations. Thus, a single process parameter or an interaction is significant if the p-value is less than 0.05. Minitab R.16 and Statistica V.7 software tools were adopted for the analysis. After the tests, the samples were cut, included in epoxy resin and then polished using abrasive paper of grit size up to P2500 (Standard ISO 6344). Then, images of the kerf sections were taken by optical microscopy (Zeiss Axioskop 40 and Hirox KH 8700) and the geometry was measured according to the UNI EN ISO 12584 and ISO 9013:2002 standards. In particular, the kerf width at the inlet of the beam (top kerf, Tk), and at the exit of the beam, (bottom kerf, Bk), the angularity tolerance (u) and the dross height (Dh) were measured. Figure 4 shows a scheme of the kerf section and how Tk, Bk, u and Dh were adopted as response variables for the kerf geometry.

Table 8 ANOVA results for geometrical parameters, p-value

Control factor Source	Tk [mm]	Bk [mm]	Ta [deg]	u [mm]	Dh [mm]
Dr	*0.000*	*0.000*	*0.000*	0.431	0.272
D [ms]	0.115	*0.000*	*0.000*	*0.000*	*0.000*
Sl [%]	0.562	0.484	0.232	0.279	0.140
Dr × D	*0.047*	*0.034*	*0.002*	*0.000*	0.140
Dr × Sl	0.567	0.353	0.165	*0.009*	0.242
Sl × Dr	0.816	0.922	0.975	0.256	0.840
Dr × D × Sl	0.879	0.111	0.199	0.262	0.063

Significant factors and interations are hilighted by italic text.

In addition, after measuring, the taper angle (Ta) was calculated via the following equation:

$$\mathrm{Ta} = \tan^{-1}\left[(\mathrm{Uk}-\mathrm{Dk})\Big/(2\cdot t)\right] \tag{4}$$

where, in the equation, t is the sheet thickness.

The taper angle and the angularity tolerance have a similar meaning. However, while the taper angle is affected by the kerf width values, the angularity tolerance is not influenced by this issue and it is more effective in the description of the angularity in the inner part of the kerf.

In order to qualify the kerf quality, the following roughness parameters were adopted as response variables: arithmetic mean surface roughness (Ra), maximum height of the profile (Rt), mean width of profile elements (RSm), according to the ISO 1302:2002 standard. The roughness parameters were measured by using a 3D Surface Profiling System (Talysurf CLI 2000 from Taylor Hobson), equipped with an inductive gauge and a 2-μm radius diamond stylus. Profiles of 5 mm in length were acquired on the cut surface, along the cutting direction, at 0.2 mm from the top kerf (obtaining the roughness parameters Ra_T, Rt_T and RSm_T) and 0.2 mm from the bottom kerf (obtaining the roughness parameters Ra_B, Rt_B and RSm_B) as shown in Fig. 4.

The use of two different positions for the measurement of the roughness parameters was chosen on the basis of a preliminary observation of the profiles. A variation of the surface roughness along the profile was observed: specifically, all the roughness parameters increase passing from the top to

Table 9 ANOVA results for roughness parameters, *p*-value

Control factor Source	Ra_T [μm]	Rt_T [μm]	RSm_T [mm]	Ra_B [μm]	Rt_B [μm]	RSm_B [mm]
Dr	0.918	0.730	0.267	0.301	0.676	*0.000*
D [ms]	0.596	0.154	*0.005*	0.343	0.510	*0.000*
Sl [%]	0.639	0.496	0.581	0.133	0.874	*0.031*
Dr × D	0.825	0.482	0.700	0.221	0.476	0.398
Dr × Sl	0.821	0.565	0.850	*0.001*	0.343	*0.004*
Sl × Dr	0.695	0.900	0.187	0.095	0.987	0.266
Dr × D × Sl	0.893	0.866	0.088	0.011	0.971	0.371

Significant factors and interations are hilighted by italic text.

the bottom kerf position. These observations were confirmed by the ANOVA performed on all the measured values adopting the position as covariate. However, the latter analysis was not reported for sake of briefness. During the profile acquisition, an axis resolution (data spacing) of 0.5 μm, a lateral resolution of 0.5 μm and a vertical resolution of 5 nm were used. The acquired profiles were processed using a surface analysis software (TalyMap Universal, release 3.1). The software allows acquiring the profiles and calculating the roughness parameters.

3 Experimental results and discussion

3.1 Maximum cutting speed

In Fig. 5, the maximum cutting speed is reported as a function of duration (D) for both directions (Dr). It can be observed that the maximum cutting speed linearly increases at the increase of pulse duration. Furthermore, as it was expected, it increases moving from direction 2 to direction 1. The results clearly indicate the effect of pulse duration (the maximum cutting speed decreases if D is decreased) and also clarify the choices made in the DoE development (i.e. the use of Sl).

For a real application, since the cutting pattern does not consist of straight lines and it is arranged along two or more directions, it is not advisable to use the maximum speed (i.e. the Sl along the direction 1). Nor it is conceivable to adjust the cutting speed as a function of direction. Therefore, to ensure an effective cutting on any type of geometry, the use of the lowest speed among those guaranteed in both directions is necessary. In Table 5, the process parameters (D, F, Pp and Ep), the maximum cutting speed (100 % Sl) and the absolute values of the Sl adopted for the second experimental test are reported.

3.2 Microscopical analysis and ANOVA results

In Figs. 6 and 7, the images of the section of some of the produced kerfs are reported for Dr = 1 and Dr = 2, respectively. From the figures, it can be observed that there are two typical kerf shapes. The first, corresponding to a lower pulse duration, is a V shape kerf (Figs. 6a–c and 7a–c,), the second, corresponding to a higher pulse duration (Figs. 6d–f and 7d–f), is

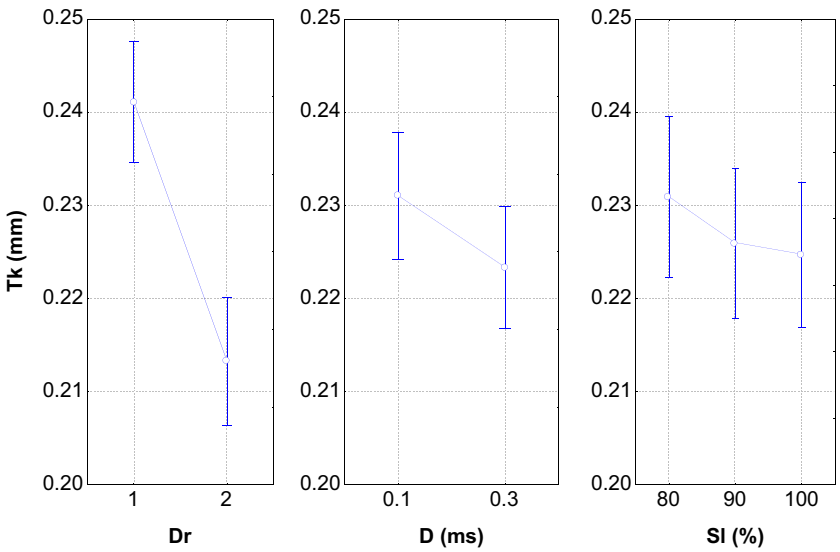

Fig. 11 Main effects plot for the top kerf width (Tk). *Vertical bars* denote 0.95 confidence intervals

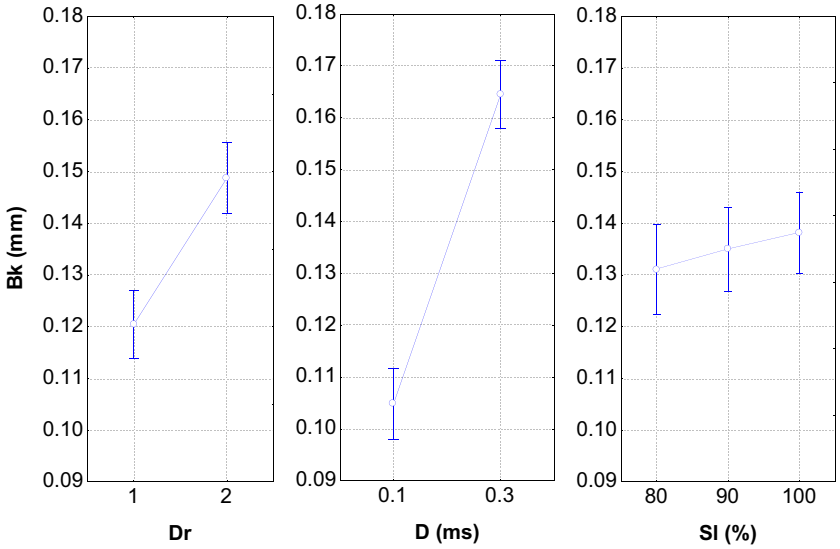

Fig. 12 Main effects plot for bottom kerf width (Bk). *Vertical bars* denote 0.95 confidence intervals

characterised by a more regular profile (i.e. perpendicular). In both cases, the material recast layer is present along the entire height of the kerf, with a thickness that increases together with the duration or moving from the top kerf to the bottom one. This material generates profile irregularity (saw tooth) in the inner part of the kerf. Moreover, the thickening of the recast layers results in dross formation. No particular changes are visible at the change of the Sl, even if a slight widening of the bottom kerf is visible at Sl decreasing. In Figs. 8 and 9, some images of the lateral surface of the kerf are reported. Although the tests were performed in PW regime and using nitrogen as assistance gas, the formation of striations has been observed on all the cut surfaces. Specifically, going from the inlet side toward the output side, three different zones are visible (Fig. 8b), each one characterised by different striation morphologies:

(i) A narrow top zone, of about 20–100 μm in height, characterised by well-defined vertical lines, due to the laser cut initiation, that involves formation of depressed melt pool on the surface of metal sheet due to the action of the gas thrust;

(ii) An intermediate zone, characterised by striations with a low angle produced by the initiation of the keyhole which rapidly penetrates into the material through material evaporation and ejection of liquid debris along with vapours. The material evaporation ceases when the laser pulse is off;

(iii) An output zone, characterised by striations tilt up to 45° (Fig. 9d), generated by the pull out effect of the gases (assistant gas and metal vapours) that drag the molten material in the direction opposite to the cutting direction.

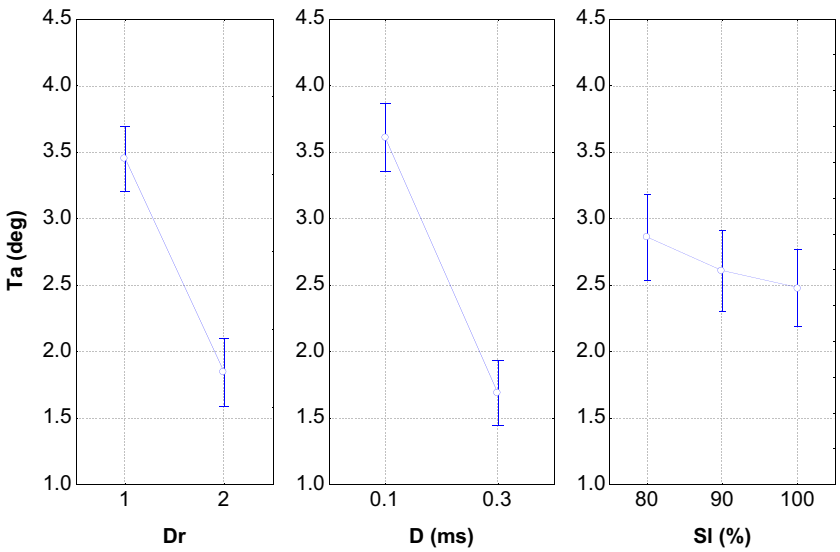

Fig. 13 Main effects plot for taper angle (Ta). *Vertical bars* denote 0.95 confidence intervals

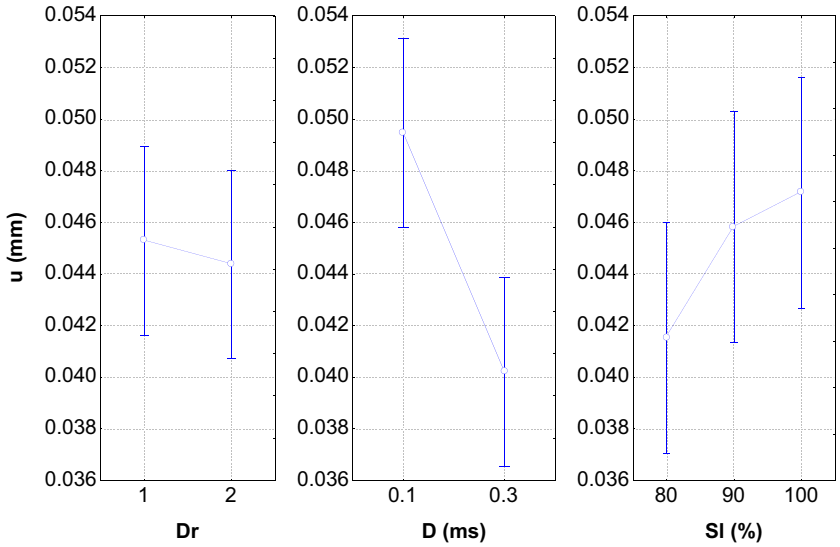

Fig. 14 Main effects plot for angularity tolerance (u). *Vertical bars* denote 0.95 confidence intervals

The surfaces are consistent to what observed in [38] where cutting tests of Ti alloy were carried out using a CW CO_2 laser. Moreover, the three types of striations are not always simultaneously present: when the laser works at low duration (0.1 ms), the first type of striations is almost absent and the third is barely visible. On the contrary, when the laser works at the highest durations (0.3 ms), the intermediate zone is absent or scarcely visible. The effect of the striation formation explains also the profile irregularity (the saw tooth geometry) in the kerf section: the molten material flow inside the kerf forming the striation that results in the section as the saw toot visible in Fig. 10, where an image of the kerf profile edge, cut at Sl = 80 %, D = 0.3 ms, Dr = 2, is reported.

The computed values of response variables for all the tests have been listed in Tables 6 and 7 for the kerf geometry and roughness, respectively. The latter separated according to the position (top and bottom). From the tables, it is possible to see that excluding the Tk, all the other response variables show a standard deviation more than the 15 % of the average values. Moreover, as expected, the average and the deviation of the roughness parameters increase passing from the top to the bottom measure positions. In order to individuate which of the process parameters mostly affect the kerf characteristics, ANOVA was performed on the measured data.

ANOVA assumes that the observations are normally and independently distributed with the same variance for each treatment or factor level. Then, before the analysis, the ANOVA assumptions have been successfully checked via graphical examination of residuals, in agreement with what reported in [35]. However, these results were not reported here

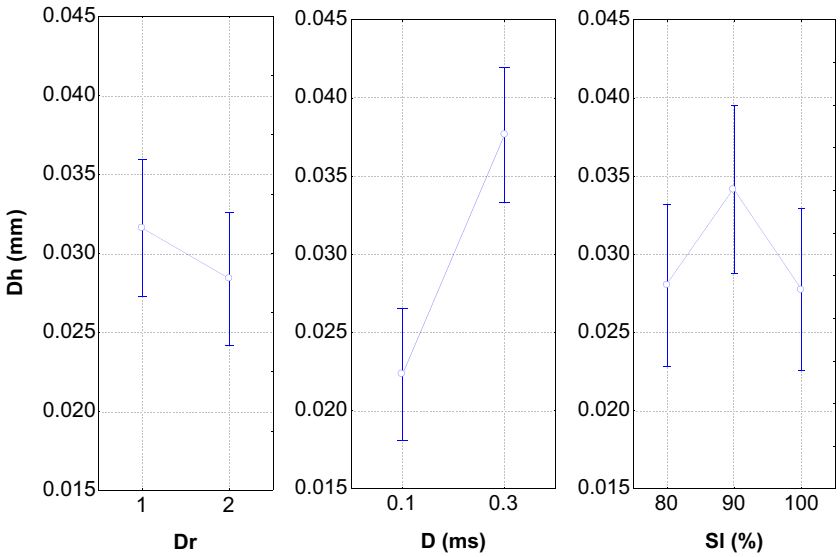

Fig. 15 Main effects plot for dross height (Dh). *Vertical bars* denote 0.95 confidence intervals

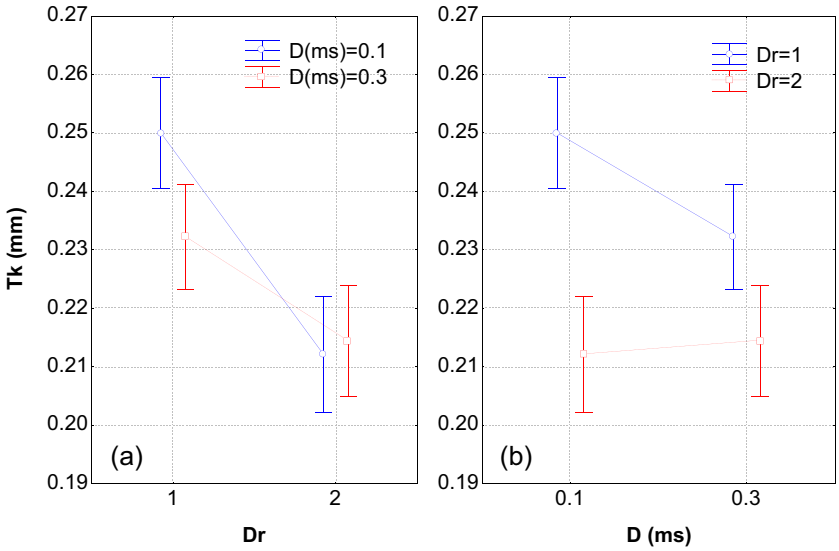

Fig. 16 Interaction plot for top kerf width (Tk). *Vertical bars* denote 0.95 confidence intervals

for sake of briefness. In Tables 8 and 9, the ANOVA results for the geometry and roughness parameters are summarized in terms of *p*-values. From Table 8, and on the basis of the assumptions ($\alpha = 0.05$), it can be observed that the direction affects both the kerf widths and the taper angle, while the duration affects the bottom kerf, the taper angle, the angularity tolerance and the dross height. The maximum cutting speed (Sl) does not affect any response variables. This is unexpected, it is probably due to the use of too close values of Sl. Regarding the two-way interaction, ANOVA indicates, as significant, the interaction Dr × D for Tk, Bk, u and Ta, and Dr × Sl for u.

As regard the roughness parameters (Table 9), Ra_T, Rt_T and Rt_B are not affected by any control factors, RSm_T is affected only by duration and RSm_B by all the control factors (Dr, D and Sl). Moreover, the ANOVA indicates as significant the interaction Dr×Sl for Ra_B and RSm_B.

The ANOVA table is a useful tool to detect the statistical significance of the process parameters and their combination. However, the table does not give any information about the "effect" of the process parameters. These aspects will be analysed, together to the technological interpretation, in the next paragraphs, by using the main effect plot and the two-factor interaction plot.

3.3 Effect of process parameters on the kerf geometry

The main effects plots and the interaction plots reported in Figs. 11, 12, 13, 14, 15, 16, 17, 18, 19 and 20 help understand the effect of the significant factors. In the main effects plots

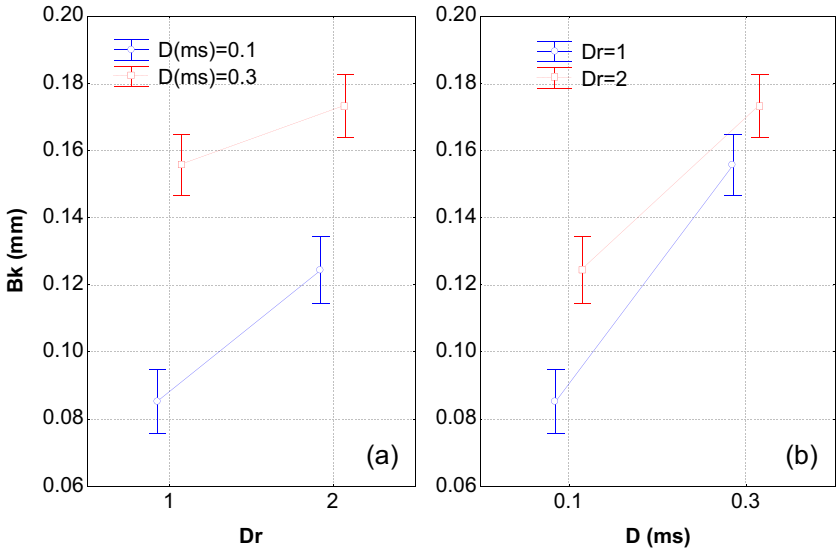

Fig. 17 Interaction plot for bottom kerf width (Bk). *Vertical bars* denote 0.95 confidence intervals

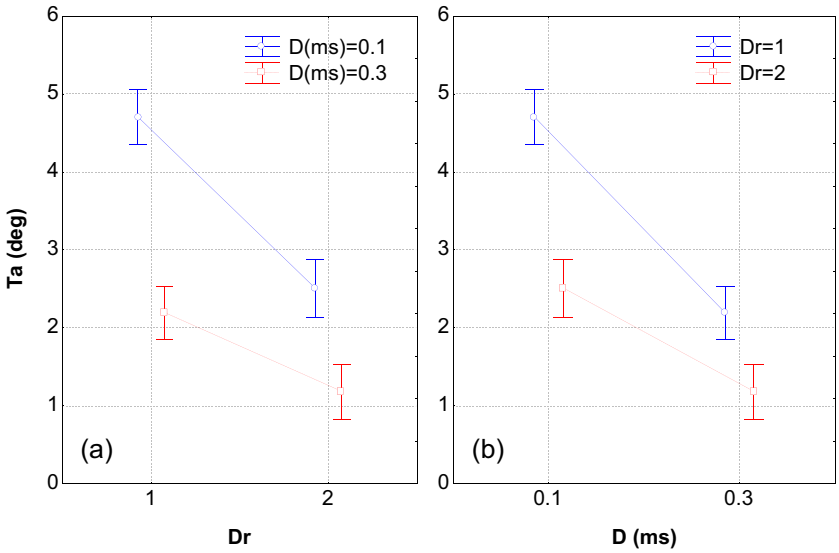

Fig. 18 Interaction plot for taper angle (Ta). *Vertical bars* denote 0.95 confidence intervals

(Figs. 11, 12, 13, 14 and 15), the significant factors are highlighted using continuous lines. In the interaction plots (Figs. 16, 17, 18, 19 and 20), only the statistically significant interactions are reported.

In Fig. 11, the main effects plot for Tk shows that the top kerf decreases moving from direction 1 to 2. As long as the beam width is smaller along the direction 1 with respect to the direction 2, this result is unexpected. The highest kerf width, obtained in direction 1, is probably due to the fact that in this direction the laser beam works at a nominal Sl lower than the true Sl. As a matter of fact, it is working at a Sl that is about 25 % less than the one corresponding to this direction (Fig. 5). Consequently, the molten material increases and the top kerf is enlarged. The latter effect is more evident when the duration has a low value, as visible in the two-way interaction plot of Fig. 16. Under these conditions, both peak power and interaction time are reduced, and the laser shows more difficulty in cutting the sheet.

The opposite happens for the bottom kerf, Fig. 12: the high amount of molten material produced, as the laser beam travels along direction 1, tends to solidify at the bottom of the kerf, because of the high thermal conductivity of the aluminium alloy, thus reducing the bottom kerf width. It is worth noting that for Bk, the overall variation of the width due to the direction change is lower than the one for Tk. The effect of pulse duration on Bk is due to similar phenomena, Fig. 12. An increase of pulse duration leads to a higher interaction time (during pulse on-time) and a lower number of cooling cycles (during pulse off-time). Consequently, the heat accumulates in the cutting zone producing an increase of the molten material and higher temperatures in the kerf. This helps the gas to drag the molten material out of the kerf more efficiently. The

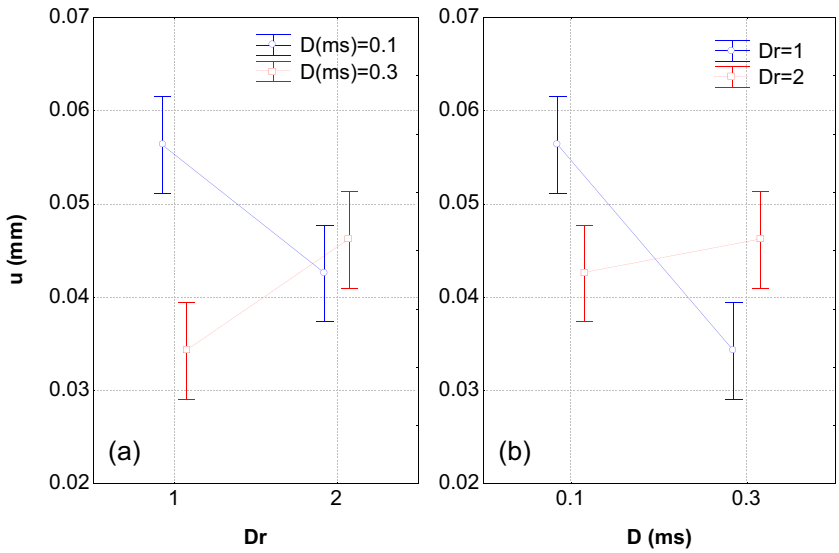

Fig. 19 Interaction plot (Dr×D) for angularity tolerance (u). *Vertical bars* denote 0.95 confidence intervals

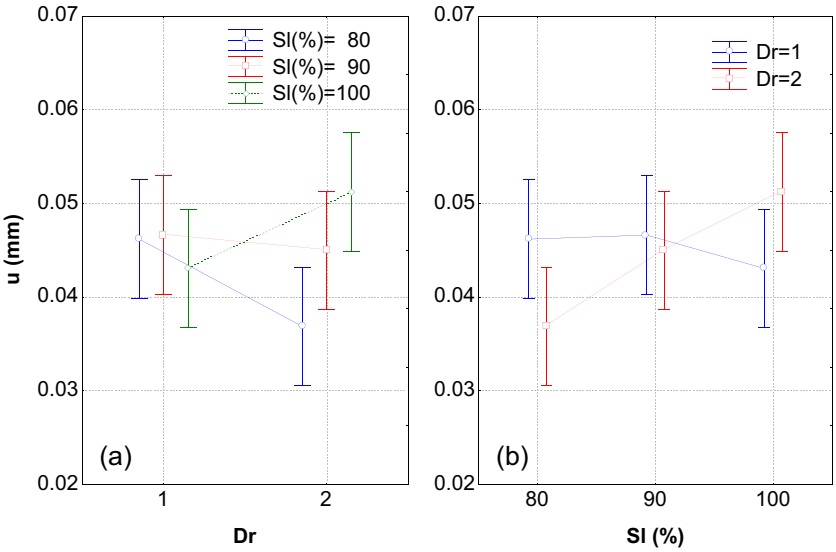

Fig. 20 Interaction plot (Dr×Sl) for angularity tolerance (u). *Vertical bars* denote 0.95 confidence intervals

contrary occurs at short duration, where the pulse energy becomes very low, so there is not much time to accumulate and diffuse heat to melt more materials. This result is consistent to what observed in [21, 38].

The effects of the direction and duration on Bk are synergistic. So, they give rise to the interaction D × Dr indicated by ANOVA (Table 8) and visible in Fig. 17. The latter can be described as follows: when the laser beam moves along direction 1, a variation of the duration produces a variation of Bk greater compared to the case in which the beam travels along direction 2 (Fig. 17b). Similarly, when the duration is set at 0.1 ms, the variation of Bk passing from direction 1 to direction 2 is greater than the one that occurs at D = 0.3 ms (Fig. 17a).

The taper angle is affected by both Tk and Bk according to the widths variations and Eq. 4, it decreases going from direction 1 to 2 and when duration increases (Fig. 13). In the latter case, the reduction of Bk, due to the duration increase, involves the reduction of Ta. Similarly to the behaviour of Tk and Bk, also in this case, the effects of direction and duration are more evident when duration is set at a low value and the beam travels along direction 1 (Fig. 18).

The behaviour of "u" partly reproduces the trend of Ta (Fig. 14), except for the fact that it is insensible to the direction and that the interaction Dr × Sl is reported as significant. The angularity tolerance u decreases at the increase of the duration thanks to the Bk widening that occurs at the D increasing. The insensibility to Dr can be justified considering the interaction

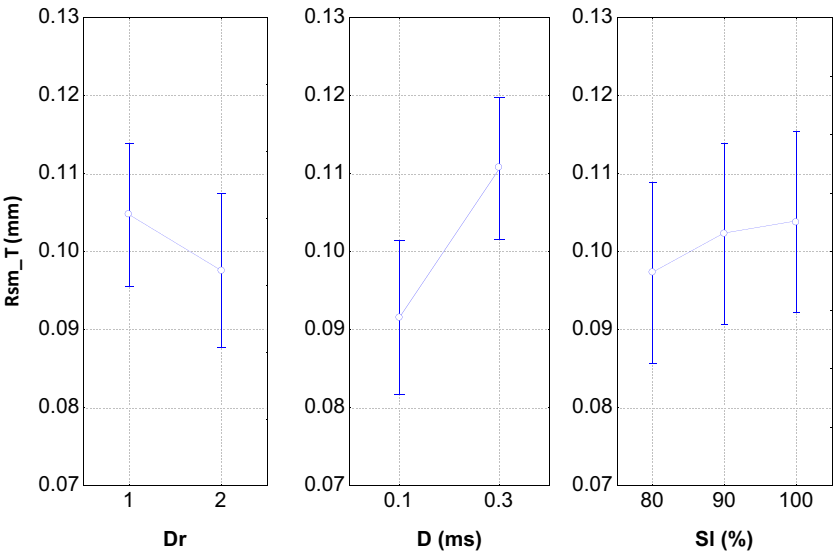

Fig. 21 Main effects plot for mean width of profile elements measured at the top kerf (RSm_T). *Vertical bars* denote 0.95 confidence intervals

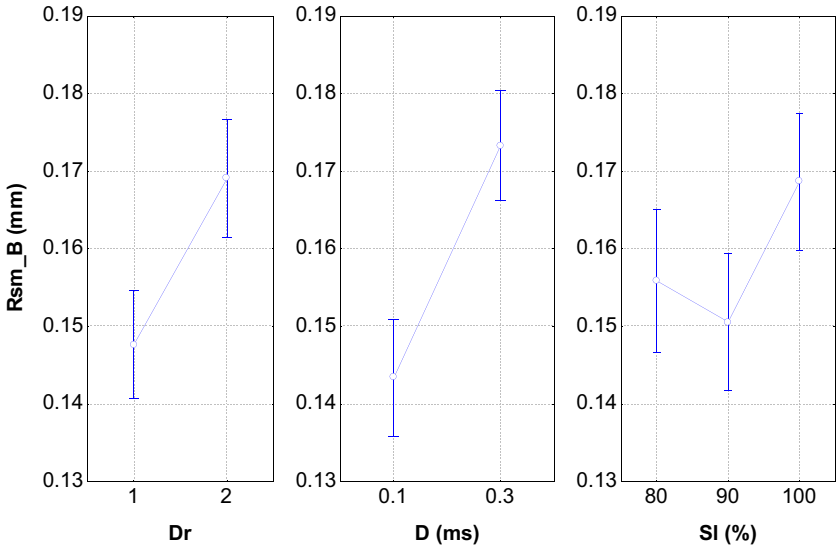

Fig. 22 Main effects plot for mean width of profile elements measured at the bottom kerf (RSm_B). *Vertical bars* denote 0.95 confidence intervals

plot Dr × D and Dr × Sl for u, as shown in Figs. 19 and 20, respectively. From the figures, it is possible to see the presence of anti-synergic interactions: at low durations, u tends to decrease going from direction 1 to 2, while at high durations the opposite happens (Fig. 19a). Figure 20a shows that at the increase of the scan speed, the slope of the response, due to the direction change, changes from a negative value for the lowest Sl to a positive one, corresponding to the high Sl. Consequently, the sum of the effects tends to hide the global effect of D. A possible interpretation of the two phenomena is that: at low duration as well as along direction 2, the laser works in the worst condition, consequently it is more sensible to any of the parameters change. Moreover, along direction 1, the angularity tolerance remains about constant, irrespective to the Sl variation.

The dross height is affected by duration only, Fig. 15, as a consequence of the previously described behaviour: as duration increases, the amount of molten material is more easily dragged and expelled out of the kerf section. However, part of the molten material tends to remain attached to the bottom edge of the kerf, thus forming the dross.

3.4 Effect of process parameters on the roughness

The main effects plots and the interaction plots of the significant control factors for the roughness parameters are reported in Figs. 21, 22, 23 and 24. As previously done, in the main effects plots (Figs. 21 and 22), the significant factors are highlighted using continuous lines. In the interaction plots

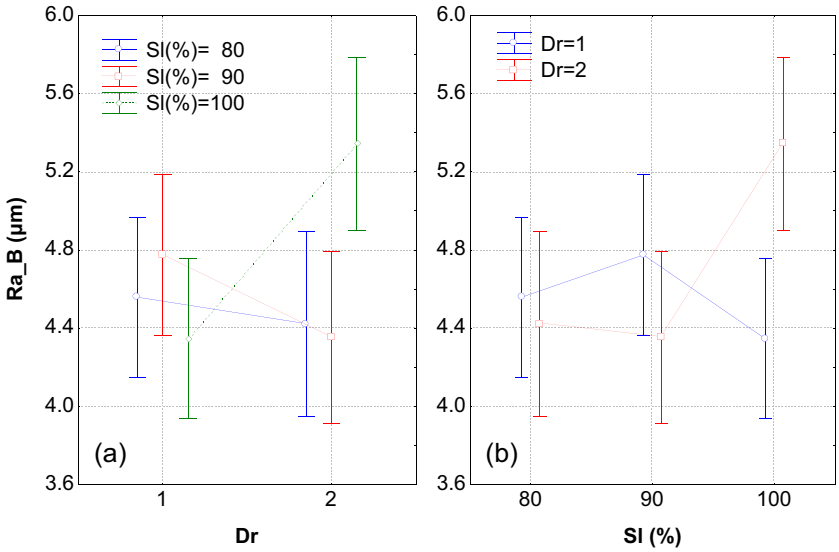

Fig. 23 Interaction plot for arithmetic mean surface roughness measured at the bottom kerf (Ra_B). *Vertical bars* denote 0.95 confidence intervals

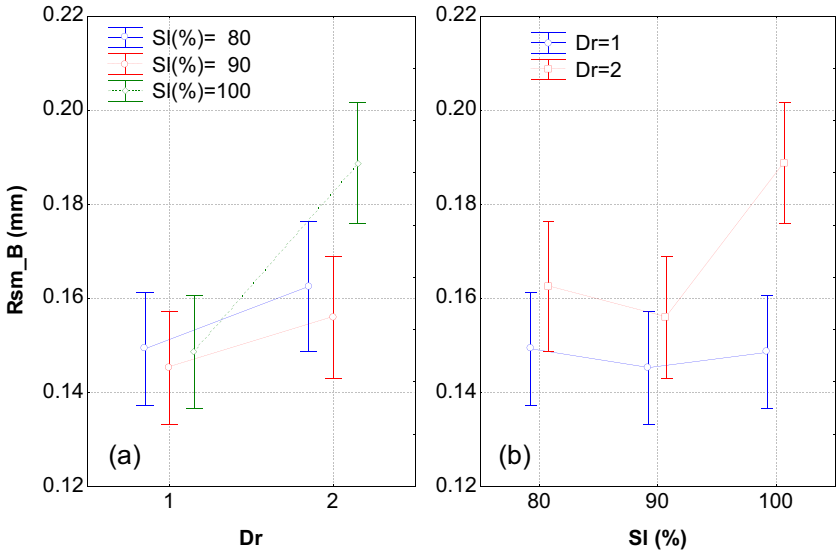

Fig. 24 Interaction plot for mean width of profile elements measured at the bottom kerf (RSm_B). *Vertical bars* denote 0.95 confidence intervals

(Figs. 23 and 24), only the statistically significant interactions are reported.

Figures 21 and 22 show that RSm parameter increases at the increase of D. In addition, RSm_B increases passing from Dr = 1 to Dr = 2 or passing from Sl = 90 % to Sl = 100 % (Fig. 22). The latter effect is mainly due to the high increase of RSm_B that occurs in direction 2, when Sl passes from 90 to 100 %, as also confirmed by the interaction plot of Fig. 24b.

The previous behaviour can be explained considering the above-mentioned observation, described in paragraph 3.2, about the mechanism of molten material formation and solidification. As previously said, the molten material quantity increases passing from direction 1 to 2 or increasing the duration. At the same time, the molten material tends to be dragged by the gases and, due to the thermal conductivity of aluminium, it cools and solidifies inside the kerf. The latter results in a covering of the primary striation that hides the original striation frequency.

Regarding the effect of Sl (Fig. 22), it is worth noting that the statistical significance is mainly due to the increase that RSm has when, along direction 2, it passes from Sl = 90 % to Sl = 100 %, as clearly visible in the interaction plot of Fig. 23. Moreover, the average values that RSm_B assumes at Sl = 100 % and Dr = 2 are independent by the duration (0.18 mm for D = 0.1 ms against 0.19 mm for D = 0.3 ms). So, it is reasonable to adduce this increase to the fact that when the beam works along direction 2 at Sl = 100 %, it works close to its limit conditions (Fig. 5). This does not happen along direction 1 because, as aforementioned, along this direction the laser beam works at a nominal Sl lower than the true Sl (Fig. 5). This is confirmed by the similar behaviour of the Ra_B roughness parameters visible in Fig. 23, where the interactions plot Dr × Sl is reported.

3.5 Discussion

In pulse wave regime, the material removal mechanism is cyclic: during the pulse on-time, the molten material is formed, while during the pulse off-time part of the molten material is ejected and part resolidified inside the kerf [38]. These phenomena are highlighted when a light-reflective and heat-conductive metal, such as aluminium, is worked.

The molten material quantity depends on the cycle width: the heat accumulated inside the kerf and the ability to eject the molten material out of the kerf change and, consequently, the kerf geometry varies. Fixed the average power (150 W), a longer duration (lower frequency) involves in a higher maximum cutting speed and thus, an improvement of process energy efficiency is obtained. At the same time, the molten material quantity tends to increase together with the temperature of the substrate, the gas drags out of the kerf the molten material more efficiently, the material removal enhance and, therefore, the kerf perpendicularity also improves. On the other hand, also the material that solidifies inside the kerf increases. The latter reduces the roughness parameter RSm, but creates a dense coating that could give problems in the long term behaviours (corrosion, fatigue, etc.).

Regarding the insensitivity of the kerf characteristic to the Sl, it is worth noting that it can be due to the closed levels adopted in the experimentation (80, 90 and 100 %). However, the use of the true speed of cutting (mm/min) instead of Sl would not have permitted a comparison between heterogeneous cutting conditions for the two duration values. In other words, since the maximum cutting speed strongly depends on the duration, any different choice would have penalized significantly either one or the other duration.

The results have also highlighted the importance of beam quality, not much in terms of absolute quality of the cut (since

it is already well known!), but in terms of variability of the kerf characteristics as the cutting direction changes. This clearly indicates that in a shop floor, when a multimode laser source is adopted and small and complex 2D geometries with tight tolerance and low roughness are required, also this variability has to be taken into account during the process optimization. On the basis of this observation, it can be deduced that the use of the direction as control factor has proved an effective choice.

A possible solution to reduce the variability of kerf characteristics would be the use of a source with a Gaussian distribution and a M^2 as low as possible. The latter is easily achieved adopting a fibre laser, such as the recent QCW source (quasi continuous wave source), or by applying a pinhole to a multimode Nd:YAG. Unfortunately, the latter technique involves in a high average power reduction and thus in a reduction of the already low energy efficiency of this kind of laser.

Concerning the roughness, it was demonstrated that, although it is possible to obtain low roughness values (up to 2.51 and 3.66 μm in terms of Ra_T and Ra_B respectively), since the ANOVA does not indicate any significant control factor, it is hard to control the roughness variability.

4 Conclusions

Laser cutting tests were performed on 1 mm thick aluminium alloy 6061-T6 sheets adopting a 150 W multimode pulsed Nd:YAG laser. Two experimental test plans were developed and performed. The first was used to measure the maximum cutting speed at the maximum average power. In the second test series, the effects of beam travel direction, pulse duration and cutting speed (selected as a percentage of the maximum cutting speed) on the kerf geometry and quality were investigated by means of ANOVA. For the adopted source and under the investigated condition, the main results can be summarized as follows.

The maximum cutting speed varies in the range 450–1200 mm/min depending on beam travel direction and pulse duration. It increases with longer pulse duration and when the laser beam travels along the major axis of the "quasi-elliptical focus footprint".

The large difference in terms of maximum cutting speed found for the two durations has suggested the use of the maximum speed percentage instead of the true cutting speed. This choice was effective because it allowed comparing very different process conditions.

The beam travel direction affects both the kerf widths and the taper angle.

The pulse duration affects the bottom kerf, the taper angle, the angularity tolerance and the dross height. From a practical point of view, a nearly perpendicular kerf ($Ta < 4°$) can be obtained adopting a long pulse duration. Under this condition, a dross height lower than 40 μm is obtained.

The surface quality is mainly affected by how much molten material is produced and how it solidifies because the striations morphology depends from the latter mechanism. All the roughness parameters increase passing from the top to the bottom kerf position, since the molten material tends to solidify at the kerf bottom. Ra and Rt are not influenced by the control factors. The results show that a Ra_B value in the range 3.6–4.6 μm and a Rt in the range 23–74 μm could be obtained.

On the other hand, RSm_B is the only roughness parameter affected by all the control factors. In particular, RSm_B increases when the laser beam travels along direction 2 and with longer pulse durations. From the interaction plot, the effect of Sl is evident only when the beam travels close to 100 % of the real critical speed.

The results have also highlighted the importance of the beam travel direction and the use of the direction as control factor. As a matter of fact, when a multimode laser is adopted, the process optimisation must take into account also this parameter. Otherwise, the risk to obtain results that have no counterpart in practice is concrete.

Acknowledgments The authors gratefully acknowledge the CIRTIBS Research Centre of the University of Naples Federico II and MBDA Italia Spa for providing the equipment, the materials and the technical support necessary to the development of this research work.

References

1. Stournaras A, Stavropoulos P, Salonitis K, Chryssolouris G (2009) An investigation of quality in CO_2 laser cutting of aluminium. Cirp J Manuf Sci Technol 2:61–69. doi:10.1016/j.cirpj.2009.08.005
2. Kalpakjian S, Schmid SR (2013) Manufacturing engineering and technology (7th Edition), Prentice Hall, USA, ISBN: 9780133128741
3. Salonitis K, Stournaras A, Tsoukantas G, Stavropoulos P, Chryssolouris G (2007) A theoretical and experimental investigation on limitations of pulsed laser drilling. J Mater Process Technol 183:96–103. doi:10.1016/j.jmatprotec.2006.09.031
4. Dubey AK, Yadava V (2008) Laser beam machining—a review. Int J Mach Tools Manuf 48:609–628. doi:10.1016/j.ijmachtools.2007.10.017
5. Astarita A, Genna S, Leone C, Memola CMF, Paradiso V, Squillace A (2013) Ti-6Al-4V cutting by 100W fibre laser in both CW and modulated regime. Key Eng Mater 554-557:1835–1844. doi:10.4028/www.scientific.net/KEM.554-557.1835
6. Morace RE, Leone C, De Iorio I, (2006) Cutting of thin metal sheets using Nd:YAG lasers with different pulse duration. In: PROC OF SPIE, 6157 workshop on laser applications in Europe, Dresden, Germany, 23 November 2005. doi:10.1117/12.661182
7. Astarita A, Genna S, Leone C, Minutolo F, Paradiso V, Squillace A (2014) Laser cutting of aluminium sheets with a superficial cold spray titanium coating. Key Eng Mater 611-612:794–803. doi:10.4028/www.scientific.net/KEM.611-612.794
8. Lutey AHA, Fortunato A, Ascari A, Carmignato S, Leone C (2015) Laser cutting of lithium iron phosphate battery electrodes:

characterization of process efficiency and quality. Opt Laser Technol 65:164–174. doi:10.1016/j.optlastec.2014.07.023
9. Tonshoff HK, Emmelmann C (1989) Laser cutting of advanced ceramics. Cirp Ann Manuf Technol 38:219–222. doi:10.1016/S0007-8506(07)62689-4
10. Quintero F, Pou J, Lusquiños F, Boutinguiza M, Sot R, Pérez-Amor M (2001) Nd:YAG laser cutting of advanced ceramics. Proc SPI0045 4419:756–760. doi:10.1117/12.437083
11. Leone C, Pagano N, Lopresto V, De Iorio I (2009) Solid state Nd:YAG laser cutting of CFRP sheet: influence of process parameters on kerf geometry and HAZ, 17th Int. Conf. on Composite Materials - ICCM-17, July 27-31, Edinburgh, UK, Code 85394, pp. 1–10
12. Leone C, Genna S, Tagliaferri V (2014) Fibre laser cutting of CFRP thin sheets by multi-passes scan technique. Opt Lasers Eng 53:43–50. doi:10.1016/j.optlaseng.2013.07.027
13. Chen SL (1999) The effects of high-pressure assistant-gas flow on high-power CO_2 laser cutting. J Mater Process Techol 88(1):57–66. doi:10.1016/S0924-0136(98)00402-6
14. Lamikiz A, Lacalle LNL, Sanchez JA, Pozo D, Etayo JM, Lopez JM (2005) CO_2 laser cutting of advanced high strength steels (AHSS). Appl Surf Sci 242:362–368. doi:10.1016/j.apsusc.2004.08.039
15. Rajaram N, Ahmad JS, Cheraghi SH (2003) CO_2 laser cut quality of 4130 steel. Int J Mach Tools Manuf 43:351–358. doi:10.1016/S0890-6955(02)00270-5
16. Karatas C, Keles O, Uslan I, Usta Y (2006) Laser cutting of steel sheets: influence of workpiece thickness and beam waist position on kerf size and striation formation. J Mater Process Technol 172:22–29. doi:10.1016/j.jmatprotec.2005.08.017
17. Chryssolouris G (1991) Laser machining: theory and practice (Mechanical Engineering Series). Springer, New York. ISBN 978-0387974989
18. Steen WM, Mazumder J (2010) Laser material processing, IVth edn. Springer-Verlag, London. ISBN 9781849960618
19. Ready JF, Farson DF, (2001) LIA Handbook of Laser Materials Processing, Springer-Verlag Berlin and Heidelberg GmbH & Co. U.K., ISBN: 978-3-540-41770-5
20. Thawari G, Sundar JKS, Sundararajan G, Joshi SV (2005) Influence of process parameters during pulsed Nd:YAG laser cutting of nickel-base superalloys. J Mater Process Technol 170:229–239. doi:10.1016/j.jmatprotec.2005.05.021
21. Ghany KA, Newishy M (2005) Cutting of 1.2 mm thick austenitic stainless steel sheet using pulsed and CW Nd:YAG laser. J Mater Process Technol 168:438–447. doi:10.1016/j.jmatprotec.2005.02.251
22. Araújo D, Carpio FJ, Méndez D, García AJ, Villar MP, García R, Jiménez D, Rubio L (2003) Microstructural study of CO_2 laser machined heat affected zone of 2024 aluminum alloy. Appl Surf Sci 208-209(1):210–217. doi:10.1016/S0169-4332(02)01375-2
23. Riveiro A, Quintero F, Lusquiños F, Pou J, Pérez-Amor M (2008) Laser cutting of 2024-T3 aeronautic aluminum alloy. J Laser Appl 20(4):230–235. doi:10.2351/1.2995769
24. Dubey AK, Yadava V (2008) Optimization of kerf quality during pulsed laser cutting of aluminum alloy sheet. J Mater Process Technol 204:412–418. doi:10.1016/j.jmatprotec.2007.11.048
25. Sharma A, Yadava V (2012) Modelling and optimization of cut quality during pulsed Nd:YAG laser cutting of thin Al-alloy sheet for straight profile. Opt Lasers Techno 44(1):159–168. doi:10.1016/j.optlastec.2011.06.012
26. Sharma A, Yadava V (2013) Modelling and optimization of cut quality during pulsed Nd:YAG laser cutting of thin Al-alloy sheet for curved profile. Opt Lasers Eng 51(1):77–88. doi:10.1016/j.optlaseng.2012.07.012
27. Ion JC (2005) Laser processing of engineering materials, principles, procedure and industrial application. Butterworth-Heinemann Ltd, Burlington, USA, ISBN: 0-7506-6079-1
28. Rajpurohit SR, Patel DM (2012) Striation mechanism in laser cutting—the review. Int J Eng Res App 2(2):457–461
29. Miyamoto I, Maruo H (1991) The mechanism of laser cutting. Weld World 29(9-10):283–294
30. Ivarson A, Powell J, Kamalu J, Magnusson C (1994) The oxidation dynamics of laser cutting of mild steel and the generation of striations on the cut edge. J Mater Process Technol 40:359–374. doi:10.1016/0924-0136(94)90461-8
31. Kim BC, Kim T, Jang Y, Chung K (2001) Investigation of striation formation in thin stainless steel tube during pulsed Nd:YAG laser cutting process by Numerical analysis. Metall Mater Trans A 32(10):2623–2625. doi:10.1007/s11661-001-0052-7
32. Paschotta R (2008) Encyclopedia of laser physics and technology. 1st edition. Wiley-VCH, Berlin, ISBN: 978-3-527-40828-3
33. Leone C, Genna S, Caggiano A, Tagliaferri V, Molitierno R, (2015) An investigation on Nd:YAG laser cutting of Al 6061 T6 alloy sheet. In: 3rd CIRP global web conference on production engineering research: advancement beyond state of the art, CIRPe 2014, 3-5 June 2014, vol 28. PROCEDIA CIRP, Naples, Italy, pp. 64–69. doi:10.1016/j.procir.2015.04.012
34. Metals Handbook (1990) Vol. 2—Properties and selection: nonferrous alloys and special-purpose materials. 10th Ed., ASM International
35. Montgomery DC (2008) Design and analysis of experiments. Wiley, New York. ISBN 0471316490
36. Genna S, Leone C, Palumbo B, Tagliaferri F (2015) Statistical Approach to fiber laser microcutting of NIMONIC® C263 superalloy sheet used in effusion cooling system of aero engines. Procedia Cirp 33:520–525. doi:10.1016/j.procir.2015.06.067
37. Dittrich M, Dix M, Kuhl M, Palumbo B, Tagliaferri F (2014) Process analysis of water abrasive fine jet structuring of ceramic surfaces via design of experiment. Procedia Cirp 14:442–447. doi:10.1016/j.procir.2014.03.030
38. Rao BT, Kaul R, Tiwari P, Nath AK (2005) Inert gas cutting of titanium sheet with pulsed mode CO_2 laser. Opt Lasers Eng 43(12):1330–1348. doi:10.1016/j.optlaseng.2004.12.009